Experimental strategies for *invivo* ^{13}C NMR spectroscopy

Julien Valette, Brice Tiret, Fawzi Boumezbeur

Analytical Biochemistry 529 (2017) 216–228

Contents lists available at ScienceDirect

Analytical Biochemistry

journal homepage: www.elsevier.com/locate/yabio

Experimental strategies for *in vivo* ^{13}C NMR spectroscopy

Julien Valette [a, b, *], Brice Tiret [a, b], Fawzi Boumezbeur [c]

[a] Commissariat à l'Energie Atomique et aux Energies Alternatives (CEA), Direction de la Recherche Fondamentale (DRF), Institut d'Imagerie Biomédicale (I2BM), MIRCen, F-92260 Fontenay-aux-Roses, France
[b] Centre National de la Recherche Scientifique (CNRS), Université Paris-Sud, Université Paris-Saclay, UMR 9199, Neurodegenerative Diseases Laboratory, F-92260 Fontenay-aux-Roses, France
[c] Commissariat à l'Energie Atomique et aux Energies Alternatives (CEA), Direction de la Recherche Fondamentale (DRF), Institut d'Imagerie Biomédicale (I2BM), NeuroSpin, F-91190 Gif-sur-Yvette, France

ARTICLE INFO

Article history:
Received 11 March 2016
Received in revised form
24 May 2016
Accepted 4 August 2016
Available online 8 August 2016

Keywords:
^{13}C
Magnetic resonance spectroscopy
Metabolism
In vivo
Magnetic resonance methodology

ABSTRACT

In vivo carbon-13 (^{13}C) MRS opens unique insights into the metabolism of intact organisms, and has led to major advancements in the understanding of cellular metabolism under normal and pathological conditions in various organs such as skeletal muscles, the heart, the liver and the brain. However, the technique comes at the expense of significant experimental difficulties. In this review we focus on the experimental aspects of non-hyperpolarized ^{13}C MRS *in vivo*. Some of the enrichment strategies which have been proposed so far are described; the various MRS acquisition paradigms to measure ^{13}C labeling are then presented. Finally, practical aspects of ^{13}C spectral quantification are discussed.

1. Introduction

In vivo carbon-13 (^{13}C) magnetic resonance spectroscopy has emerged about thirty years ago as a unique technique to study metabolism in intact organisms, and since then has generated important knowledge about cellular metabolism in various organs such as skeletal muscles, the heart, the liver and, maybe most importantly, the brain, with major advancements in the understanding of cerebral energy metabolism, neuron-astrocyte compartmentation and cooperation, and glutamatergic neurotransmission (see Refs. [1,2] for recent review about ^{13}C MRS in the brain). The basic principles underlying the approach are quite simple. ^{13}C, the only stable isotope of carbon having a nuclear magnetic moment, has a natural abundance of only ~1.1%, so that administration of a highly ^{13}C-enriched substrate will yield an unambiguous ^{13}C MRS signal increase. Unlike techniques based on radioactive isotopes, such as positron emission tomography or autoradiography, MRS offers the unparalleled ability to chemically resolve the origin of the signal. It allows precisely tracking the metabolic fate of administered ^{13}C-labeled substrates, i.e. specifically identifying which metabolites are being labeled, and at what atomic positions. This unique chemical specificity unfortunately comes at the expense of detection sensitivity when compared to radioisotope techniques, with detection thresholds being of the order of the millimolar (mM). This has been driving many methodological efforts to improve acquisition strategies to enhance measurement's temporal or spatial resolution. Once methodological challenges have been adequately addressed, one of the great strengths of MRS is the possibility to get a quantitative measurement of ^{13}C labeling, either in terms of fractional enrichment (the ratio between labeled and total pools) or of absolute ^{13}C concentration, making possible the estimation of metabolic fluxes *via* metabolic modeling.

In this paper we review experimental strategies for ^{13}C MRS *in vivo*. We first introduce some of the enrichment strategies which have been proposed so far. Then, the various MRS acquisition paradigms to measure ^{13}C labeling are presented. Finally, we discuss some practical aspects of ^{13}C quantification on spectra.

* Corresponding author. Commissariat à l'Energie Atomique et aux Energies Alternatives (CEA), Bâtiment 61, 18 Route du Panorama, 92260 Fontenay-aux-Roses, France.
E-mail address: julien.valette@cea.fr (J. Valette).

http://dx.doi.org/10.1016/j.ab.2016.08.003
0003-2697/

2. Strategies for ^{13}C infusion and labeling of endogenous metabolites

Before going through the variety of ^{13}C-labeled substrates and infusion strategies which can be used to enrich metabolic byproducts, we shall briefly mention that natural abundance ^{13}C MRS can be of interest in a limited number of cases, essentially when the increased spectral resolution compensates for the low detection sensitivity, as compared to ^{1}H MRS. Some notable cases are fatty acids in adipose tissue [3,4] and, due to the high glycogen concentration in these organs, glycogen detection in muscle and liver (where overlap with lipid signal is avoided using ^{13}C detection) [5–8].

In most situations, natural abundance signal will not be sufficiently informative, or even detected. The typical experimental design instead consists in administering ^{13}C-labeled substrates (orally or intravenously) and observing the subsequent labeling of metabolic byproducts. “Observing the subsequent labeling” may refer to the sole observation of what atomic positions are enriched at some point in time (usually at steady-state), which might bring information about the reactions at stake and possibly about their relative importance, or in addition to the measurement of the dynamics of ^{13}C incorporation, which can provide quantitative measurement of reaction rates (in μmol/g/min) using metabolic modeling. Intravenous (i.v.) infusion will be generally preferred in the latter case, in order to quickly reach a high ^{13}C enrichment in the plasma and maintain it at stable level over a few hours (the typical time-scales to approach isotopic steady-state and to extract relevant reaction rates using metabolic modeling). In some other situations, e.g. when reaction rates at stake are too low to allow for continuous i.v. administration, or when i.v. infusion presents practical difficulties, oral administration can be more adapted (e.g. see Ref. [9] for comparison between oral and intravenous administration, and [10] for oral administration in a clinical context). In all cases, it is usually desirable to perform frequent blood sampling in order to determine the plasma concentration of labeled substrates, which is very important for proper interpretation (to say nothing of metabolic modeling) of ^{13}C MRS data. This can also help evaluating label recycling, i.e. ^{13}C-labeled metabolites being released into the bloodstream before being taken up again and re-used by organs, which is likely to occur during long infusion times. As examples, let's mention the infusion of [2-^{13}C]acetate or [3-^{13}C]lactate [11], which result in the labeling of blood glucose *via* gluconeogenesis in the liver, or the infusion of labeled glucose leading to the labeling of blood lactate.

We shall now briefly review different kinds of studies which have been performed using ^{13}C. Instead of organizing this section according to the different labeled substrates which have been used in the past, we propose to follow an organization based on the different metabolic questions that can be addressed (although there is some overlap between some of these questions).

2.1. Substrate-specific metabolism

^{13}C MRS is a tool of choice to assess how specific substrates are metabolized by organs, and what is their metabolic fate. The labeling patterns of a given observed metabolite may help elucidate what reactions/enzymes link the infused labeled-substrate to the observed metabolite. Furthermore, different substrates can be infused simultaneously, leading to different and specific labeling patterns of the same molecule, i.e. different “isotopomers”. Isotopomers are the different sets of atomic positions simultaneously labeled on individual molecules, whose detection is made possible on ^{13}C spectra by ^{13}C-^{13}C scalar J-coupling (mostly between immediate neighbors), which results in the splitting of ^{13}C resonances. Comparison between the amounts of these different isotopomers may provide unique information about the relative importance of metabolic fluxes connecting substrates to observed metabolites. In that context, a large variety of ^{13}C-labeled substrates can be administered. As non-exhaustive examples beyond glucose, let's mention the metabolic fate of (and competition between) [3-^{13}C]alanine and [2-^{13}C]ethanol in a pioneer work performed in perfused mouse livers [12]; [1,3-$^{13}C_2$]butyrate for ketone body production in the rat liver [13]; [U-$^{13}C_3$]glycerol, [U-$^{13}C_6$]glucose, and [U-$^{13}C_3$]lactate to evaluate the relative contribution of these substrates to acylglycerols after passage through the citric acid cycle in the liver [14]; [2-^{13}C]acetate, [3-^{13}C]lactate, [3-^{13}C]pyruvate and [3-^{13}C]propionate and their incorporation into tricarboxylic acid cycle in perfused hearts [15–17]; uniformly labeled [U-$^{13}C_3$]glycerol and [U-$^{13}C_3$]lactate to examine their contribution to acylglycerols and glycogen formation in the skeletal muscle [18]; metabolism of [1,2-$^{13}C_2$]acetate or [2-^{13}C]acetate in the brain [19–21]; [U-$^{13}C_4$]3-hydroxybutyrate in rat brain [22]; [3-^{13}C] and [2-^{13}C]pyruvate to study pyruvate metabolism in the brain [23]; [3-^{13}C]lactate to study cerebral lactate metabolism [11,24,25]; and [U-$^{13}C_5$]glutamine in the mouse brain to characterize glutamine uptake by the brain [26]. Examples of the different labeling patterns obtained in the Human brain when infusing [3-^{13}C]lactate, [1-^{13}C]glucose or [2-^{13}C]acetate are shown in Fig. 1.

It should be noted that these substrates usually have to be administered at high, non-physiological doses. Although this is a problem which is general to ^{13}C studies, it is particularly acute when the goal of the study is to determine how (in which proportions and at what rate) organs feed on specific substrates which may be only present at very low concentrations under physiological conditions, such as acetate.

2.2. Glycogen content and turnover

Glycogen is a large polymer of glucose residues, which can be readily mobilized to regenerate glucose and maintain blood-glucose levels, or rapidly provide energy during activity. The study of glycogen formation has been originally performed in the liver and the brain using ingestion or infusion of glucose labeled at position C1 ([1-^{13}C]glucose), leading to the labeling of glycogen at position C1 [27–29], which resonates at 100.5 ppm on ^{13}C spectra,

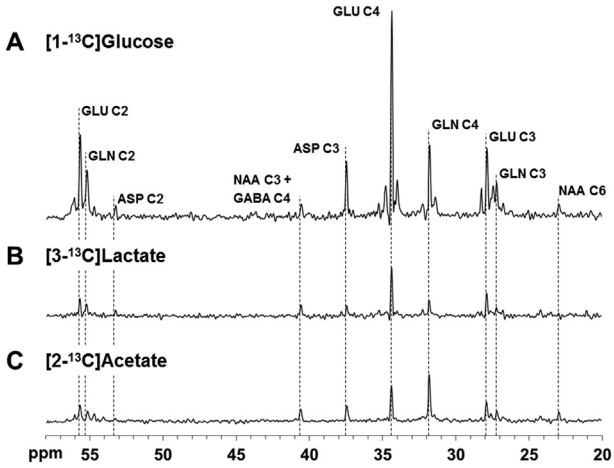

Fig. 1. Localized ^{13}C spectra acquired at 4 T from the occipito-parietal lobe of the same volunteer, at the end of a 2-h infusion of [1-^{13}C]glucose (A), [3-^{13}C]lactate (B) or [2-^{13}C]acetate (C). Vertical scaling is adjusted to differences in ^{13}C labeling for glutamate (Glu) and glutamine (Gln). It is apparent that, in contrast with glucose and lactate, acetate metabolism primarily leads to the labeling of glutamine.

well separated from other resonances. In the brain, where glycogen concentration is too low to allow detection in natural abundance (unlike in the liver and muscle), the utilization of [1-^{13}C]glucose to label glycogen and yield sufficient signal was also used to estimate glycogen content by ^{13}C MRS at isotopic steady state [30–32]. However, variations in glycogen absolute concentration and glycogen turnover rates can be difficult to disentangle when metabolism is not at steady-state, e.g. if insulin levels vary. Hence a two-step labeling strategy was recently proposed, starting with an oral [1-^{13}C]glucose administration to reach isotopic steady-state, followed by infusion of doubly labeled glucose ([1,6-$^{13}C_2$]glucose) so that fractional enrichment is maintained at position C1 of glycogen, which can be used to track concentration variations, while the dynamics of ^{13}C enrichment at position C6 of glycogen (relative to C1) will reflect turnover rates [33]. For a more comprehensive review about glycogen labeling strategies, we refer to these two recent reviews [34,35].

2.3. Tricarboxylic acid cycle

The tricarboxylic acid (TCA) cycle is of central importance for many biochemical pathways, including ATP synthesis via oxidative phosphorylation, and synthesis of amino acids such as glutamate, glutamine and aspartate. Since TCA cycle consumes large amounts of carbohydrates to meet energy demand, it is an ideal target for ^{13}C MRS studies, because high fractional enrichments of TCA cycle-derived amino acids (yielding detectable signal) can be reached in reasonable experimental times during i.v. infusion. Rather than determining the specific utilization of various substrates by TCA cycle and related fluxes (pyruvate dehydrogenase, pyruvate carboxylase, glutamate-oxaloacetate transaminase…), many studies have instead been performed to quantify these metabolic fluxes by measuring how the label flows between successive metabolic intermediates (in particular glutamate) and performing metabolic modeling of the data [12,36,37]. In this context, the ^{13}C-labeled substrate used may be of secondary importance, as long as it injects enough ^{13}C in the cycle. The main labeling routes in the cycle are represented in Fig. 2. Briefly, pyruvate (in fast exchange with lactate via lactate dehydrogenase), one of the main fuel for the TCA cycle, is decarboxylated to acetyl-CoA (AcCoA) *via* the oxidative pathway (pyruvate dehydrogenase, PDH). AcCoA enters TCA cycle by condensation with oxaloacetate (OAA), forming citrate which is subsequently converted to α-ketoglutarate (αKG), which is in turn degraded into succinate (Suc). Scrambling of ^{13}C label occurs between C1 and C4 positions of succinate, and between C2 and C3 positions, due to the symmetry of the molecule. After a few steps succinate is converted back to OAA, thus closing the cycle. Alternatively, AcCoA can be directly converted from acetate. Pyr can also enter the TCA cycle via the anaplerotic pathway, after its carboxylation to OAA, through the pyruvate carboxylase (PC). Note that, unlike PDH, PC injects new carbon skeletons in TCA cycle, i.e. it replenishes TCA cycle intermediates. Although TCA cycle intermediates are in too low concentration for *in vivo* detection by MRS, some of them are in exchange with concentrated amino-acids which can be detected (in the mM range): αKG is in exchange with Glu (through aspartate aminotransferase and glutamate dehydrogenase), OAA is in exchange with Asp (through aspartate aminotransferase).

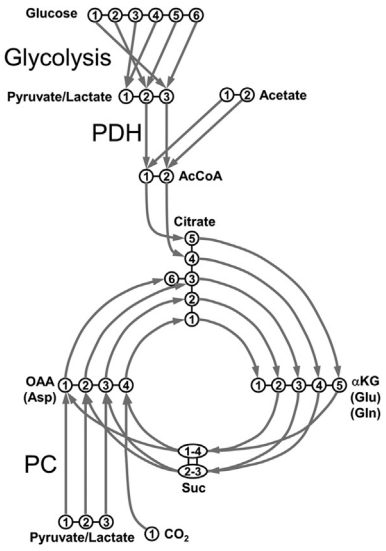

Fig. 2. Main labeling pathways associated with the tricarboxylic acid cycle. AcCoA: acetyl-CoA; αKG: α-ketoglutarate; Asp: aspartate; Gln: glutamine; Glu: glutamate; OAA: oxaloacetate; Suc: succinate; PC: pyruvate carboxylase; PDH: pyruvate dehydrogenase.

The liver has received early attention, with a comprehensive study investigating the labeling of various metabolites, including glutamate and glutamine, following infusion of [3-^{13}C]alanine in perfused mouse livers, providing qualitative results about pyruvate carboxylase and pyruvate dehydrogenase [12]. The heart followed soon after, with observation of glutamate labeling following [2-^{13}C] acetate infusion in perfused hearts [15]. As far as we know, the first truly quantitative study of TCA cycle rate based on rigorous metabolic modeling was performed in perfused hearts using [2-^{13}C]acetate and [3-^{13}C]pyruvate [36], followed by other quantitative studies using substrates such as glucose and 3-hydroxybutyrate [38]. In the brain, the main fuel for TCA cycle is glucose, which is broken down to pyruvate during glycolysis before entering the TCA cycle, so that labeled glucose has been used in most studies since the beginning [37] (mostly [1-^{13}C] and [1,6-$^{13}C_2$]glucose, the advantage of the latter being that two molecules of pyruvate labeled at position C3 are generated for each molecule of glucose, leading to doubled fractional enrichment for glutamate at positions C2, C3 and C4). If indirect ^{1}H-{^{13}C} detection is used (see Section 3), cheaper [U-$^{13}C_6$]glucose can be advantageously used instead of [1,6-$^{13}C_2$]glucose, the presence of homonuclear ^{13}C coupling between glutamate C4 and C5 (following incorporation of doubly labeled AcCoA) yielding neither additional complexity nor decreased signal-to-noise ratio (SNR) on spectra.

Alternatively, infusions of [1-^{13}C]acetate [39] and [2-^{13}C]glucose [40] have been proposed to label glutamate at position C5. Since lipid signal does not overlap with glutamate C5, this approach can be advantageous for the studies of organs where the presence of large quantities of intracellular lipid would hamper glutamate C4 quantification, e.g. in the liver [39], and may also alleviate the need for localization in situations where the latter is performed mainly to suppress subcutaneous lipid signal, e.g. in the occipital cortex of the human brain when no spectroscopic localization is performed [40]. It also requires no, or weaker heteronuclear decoupling (glutamate C5 sharing no chemical bond with ^{1}H), which might be interesting in terms of power deposition for Human studies [40] (see section 2). Note that an approximately identical SNR would be reached using non-decoupled ^{13}C MRS during infusion of [1,6-$^{13}C_2$]glucose, where labeling of two pyruvates would compensate the SNR loss due to peak splitting (although at the expense of an increased spectral complexity on non-decoupled spectra, and at a higher substrate cost).

Quantitative TCA cycle studies using metabolic modeling require well-known, and preferentially stable, substrate concentration and fractional enrichment in the blood. In the case of glucose for example, preferred infusion protocol will be conducted

on fasting animals/patients and will consist in quickly reaching (within a few minutes) a glycemia increased by a factor *G* (typically ~3) by infusing labeled glucose at a high but slowly decreasing rate to avoid overshoot. Once glycemia has increased by a factor *G*, glucose fractional enrichment is (*G*-1)/*G* (typically ~70%). Then, a mixture of labeled glucose and unlabeled glucose will be continuously perfused (with a *G*-to-1 ratio to maintain blood glucose fractional enrichment at (*G*-1)/*G*). Glycemia should be frequently measured and infusion rate adjusted accordingly to maintain it around a constant value, but typical rates vary from 1 to 8 mL/kg/h with a 20% w/v glucose solution, depending on species.

2.4. Cell-specific metabolism and intercellular cycles in the brain

Understanding and quantifying the metabolic cooperation between neurons and astrocytes has inspired many ^{13}C MRS studies over the past 20 years. Metabolic models have been refined to account for these cell types, each with their own TCA cycle rate, and how they are connected by the intercellular cycles. Glutamate (Glu) is the major excitatory neurotransmitter in the mature central nervous system. As the large neuronal pool of glutamate is rapidly labeled following the oxidation of ^{13}C-labeled glucose, glutamate released by glutamatergic neurons into the synaptic cleft is taken up by high-density [Na+/K+] glutamate transporters on astrocytic end processes. It is then converted to ^{13}C-labeled glutamine by the glia-specific glutamine synthetase. Subsequently, glutamine is released into the extracellular space, taken up by neurons and converted back to glutamate by the phosphate-activated glutaminase. Infusion of labeled glucose is not optimal to quantify astrocytic TCA cycle [41]. The potential interest of using [2-^{13}C]acetate or [1,2-$^{13}C_2$]acetate, which is metabolized and converted to Acetyl-CoA exclusively in astrocytes [42], was recognized early. Indeed, the observation of glutamine (which is primarily compartmentalized in astrocytes) labeling at position C4, and then C3 and C2, during acetate infusion provides a very specific look into astrocytic TCA cycle. The subsequent transfer of label from glutamine to glutamate (mostly neuronal) can be monitored to assess glutamate-glutamine cycle. Both substrates can be infused sequentially (at several days of interval), as shown in Humans using [1-^{13}C]glucose and [2-^{13}C]acetate, to determine both neuronal and astrocytic fluxes as well as glutamate-glutamine cycle with good precision [21]. The possibility of performing double infusion ([1,6-$^{13}C_2$]glucose + [1,2-$^{13}C_2$]acetate simultaneously) has also been proposed and demonstrated in the rat brain [43]. As can be seen on Fig. 2, labeled glucose will lead to the formation of a single peak for glutamate and glutamine C4 during the first turn of the TCA cycle, while labeled acetate will lead to the formation of glutamate and glutamine doubly labeled at position C4 and C5, which in direct ^{13}C detection will result in a doublet for glutamate/glutamine C4 due to homonuclear coupling, leading to the unambiguous separation of both labeling sources of glutamate C4 in a single MRS measurement (see Section 3). Alternatively, determination of pyruvate carboxylase has been proposed using [2-^{13}C] glucose [44,45], which is degraded into [2-^{13}C]pyruvate. Indeed, metabolism of [2-^{13}C]pyruvate through pyruvate dehydrogenase leads to the formation of [5-^{13}C]glutamate, while through astrocytic pyruvate carboxylase it leads to the formation of [3-^{13}C] glutamine, providing a clear signature for pyruvate carboxylase.

Alterations of the glutamate–glutamine cycle have been observed *in vivo* in epileptic patients [46], during healthy aging in humans [21], in anesthetized rodents [47,48], and following pharmaceutical challenges aiming at altering glutamate or GABA metabolism [49,50]. As detailed elsewhere [41], the determination of the glutamate–glutamine cycle is sensitive to fluxes significantly affecting the ^{13}C-labeling of glutamine in astrocytes, in particular the astrocytic TCA cycle, the ammonia detoxification pathway [26,51] and the oxidation of unlabeled short- and medium-chain fatty acids by astrocytes [52,53]. Also, glutamate and glutamine pool sizes in the neuronal and astrocytic compartments are other important and possibly varying parameters [54].

Since glutamate is, *via* the glutamate decarboxylase enzyme, the major precursor of γ-amino-butyric acid (GABA), the major inhibitory neurotransmitter, ^{13}C fractional enrichment time-courses of GABA can be exploited to assess its synthesis and recycling rates. However, these *in vivo* ^{13}C studies remains challenging due to the low concentration of GABA (from 1 to 3 μmol/g) and the complexity of the metabolic modeling (see Fig. 3 for a detailed representation

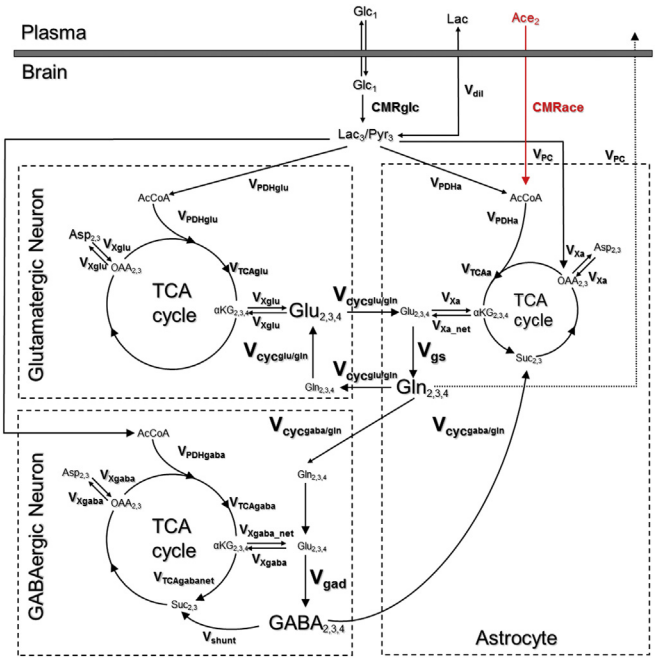

Fig. 3. Glutamatergic Neuron/Astrocyte/GABAergic Neuron three-compartment metabolic network: ^{13}C label is incorporated from [2-^{13}C]acetate or [1-^{13}C]glucose into the brain glutamate and glutamine pools. Top Left: glutamatergic neuronal compartment; Bottom Left: GABAergic neuronal compartment; Right: astroglial compartment. Abbreviations: Lac, lactate; Glc, glucose; Pyr, pyruvate; AcCoA, acetyl coenzyme A; OAA, oxaloacetate; αKG, α-ketoglutarate; Glu, glutamate; Gln, glutamine; Asp, aspartate; Suc, succinate; GABA, γ-amino-butyric acid; CMRglc, glucose consumption; CMRace, acetate consumption; V_{dil}, influx/efflux of lactate; V_{PDH}, flux through the pyruvate dehydrogenase; V_{TCA}, TCA cycle rate; V_{PC}, flux through the pyruvate carboxylase; $V_{cycglu/gln}$, glutamate/glutamine cycle flux; $V_{cycgaba/gln}$, GABA/glutamine cycle flux; V_X, mitochondrial/cytosolic glutamate/α-ketoglutarate exchange rate; V_{gs}, flux through the glutamine synthetase; V_{shunt}, GABA shunt flux in GABAergic neurons. Subscripts: **a**, **glu** and **gaba** stand respectively for astroglia, glutamatergic neuron and GABAergic neuron. The mass and isotope balance equations which describe the three-compartment models are described in details in Patel et al. [55]. [1-^{13}C]glucose is metabolized in neurons and astroglia, whereas [2-^{13}C]acetate is metabolized exclusively in astroglia (red arrow). During the [1-^{13}C]glucose infusion experiment, $^{13}C_1$-labeled glucose cross the blood brain barrier and arrives through the glycolysis at the C3 of the lactate/pyruvate pool (regrouped as a unique pool because of the very fast exchange between them through the lactate deshydrogenase), where the label enters the TCA cycle via pyruvate dehydrogenase or alternatively via pyruvate carboxylase reaction (in astroglia only). The ^{13}C-label is ultimately detected at the first turn of the TCA cycle in the C4 position of glutamate (glutamatergic and GABAergic neurons), C2 of GABA (GABAergic neurons) and C4 position of glutamine with label transfer to astroglia by neurotransmitter cycling. Then, after label scrambling by the TCA activity, C2 and C3 positions of glutamate and glutamine are labeled as well as the C3 and C4 position of GABA. During [2-^{13}C]acetate infusion experiment, the ^{13}C-label enters the astroglial TCA cycle and is rapidly detected at the C4 position of glutamine. Following the glutamate/glutamine and GABA/glutamine cycling, the C4 position of glutamate (glutamatergic and GABAergic neurons) and C2 of GABA (GABAergic neurons) are labeled.

of the network), particularly the competition between the predominant uptake of released GABA by GABAergic neurons (and subsequent conversion in succinate through the "GABA shunt" pathway) and its minor, yet significant glial uptake. As a consequence, the reported GABA-glutamine recycling rates have varied greatly [55–59]. As for the determination of the neuronal and astrocytic TCA cycle rates, the combination of labeling dynamics from multiple ^{13}C-labeled substrates is recommended for a precise estimation of Glu or GABA turnover rates.

3. ^{13}C detection

Among the many technical considerations associated with *in vivo* ^{13}C detection, one must address the actual sensitivity of the experiment, its anatomic specificity and the complexity of its set-up. Basically, two classes of MRS experiments can be considered to detect ^{13}C: direct detection, where one acquires spectra at the ^{13}C frequency (determined by ^{13}C gyromagnetic ratio $\gamma_C = 6.728 \times 10^7$ rad/s/T); or indirect detection, where one acquires spectra at the ^{1}H frequency (determined by ^{1}H gyromagnetic ratio $\gamma_H = 26.752 \times 10^7$ rad/s/T) where only signal from ^{1}H bound to ^{13}C is retained, the signal from other ^{1}H being removed by some editing technique (generally noted ^{1}H-{^{13}C}). In order to guide the reader in its future *in vivo* ^{13}C MRS endeavors, this section presents and discusses direct and indirect ^{13}C detection and localization methods as well as the hardware components needed to study metabolism using *in vivo* ^{13}C MRS.

3.1. Direct ^{13}C detection

Compared to ^{1}H MRS, ^{13}C MRS presents some specific challenges. First challenge (or opportunity depending on your point-of-view) is its low natural abundance (1.1%). A critical issue is its low intrinsic sensitivity ($\propto|\gamma|^2$ [2,60]). A significant portion of this section will present methods to circumvent this, either by enhancing ^{13}C sensitivity or by looking at the neighboring protons. Another specificity of ^{13}C is the almost systematic presence of nearby ^{1}H which leads to split resonances due to J_{CH}-coupling ($^{1}J_{CH} \approx 120–150$ Hz). On the contrary, J_{CC}-coupling is rather unlikely, at least until metabolites are labeled multiple times which occurs mostly when high ^{13}C fractional enrichments are attained. The main advantage of ^{13}C MRS is its large chemical shift range (from 160 to 200 ppm), which allows for a relatively easy discrimination between resonances of interest. However, this favorable spectral resolution comes at the cost of significant chemical shift displacement errors for direct ^{13}C localization sequences. One additional difference between ^{1}H and ^{13}C MRS is the difficulty to rely on an internal reference of concentration (see Section 4). ^{13}C MRS also suffers from relatively long T_1 relaxation times, since long T_1 limit the recovery of magnetization between each repetition, thus reducing SNR (the T_1-dependency of SNR can be approximated by an inverse square-root relationship [61]). This is particularly true for the carboxylic carbons, leading to some difficulties regarding the quantification of these signals. However, the very long T_1 (up to several dozens of seconds) of these proton-free carbons are rather interesting for ^{13}C hyperpolarized approaches.

3.1.1. Specific absorption rate

Current international guidelines (IEC 60601-2-33) states that MR studies should not expose Humans to more energy (SAR) than 3.2 W/kg (for the head) or 4 W/kg (for the body) averaged over 6 min or 10 W/kg in any 10 g in order to avoid a tissue temperature rises above 1 °C. Even if these SAR limits are rather conservative for volume coils, they are much more relevant when surface coils are used [62]. Consequently, it is critical to properly calibrate both transmission channels to minimize the RF power needed [63].

3.1.2. Non-localized and OVS-localized ^{13}C detection

For some ^{13}C MRS studies, localization is not required. This is obviously the case for experiments on cell cultures, biopsies or perfused organs. One can also perform *in vivo* ^{13}C MRS using the sensitivity profile of its surface coil to "localize" the ^{13}C signal, using a simple pulse-acquire sequence. Due to the strong lipid signal at 34.4 ppm which overlaps with resonances of interest (Fig. 4A), some localization is usually achieved by outer-volume suppression (OVS) bands [64], possibly combined with a selective inversion of the lipid signal at 34.4 ppm. This approach has been applied to study muscle and liver metabolism in particular for the investigation of muscle disorders and diabetes [65–68]. It is effective for detecting metabolites with short T_2 relaxation times such as glycogen [29,69–71].

3.1.3. Nuclear Overhauser Effect

In order to enhance ^{13}C sensitivity, one can use the Nuclear Overhauser Effect (nOe) [72]. In direct ^{13}C NMR, if one irradiates protons that are dipolar-coupled with ^{13}C nuclei, their ^{13}C thermodynamic equilibrium polarization is increased via cross-relaxation. If dipolar relaxation were the sole relaxation mechanism, the ^{13}C signal could be enhanced by a factor $1 + (\gamma_H/2\gamma_C) = 2.988$. In practice, dipolar relaxation is only one of several longitudinal relaxation mechanisms, leading to enhancements in the 1.3 to 2.9 range.

3.1.4. Broadband ^{1}H decoupling

Broadband ^{1}H decoupling allows removing the splitting of ^{13}C multiplet resonances due to the coupling with ^{1}H nuclei. It is achieved through the application of a train of RF pulses at the ^{1}H frequency during the ^{13}C acquisition. Each of these short RF pulses aims at refocusing the J_{CH} scalar coupling evolution over few acquisition points, leading to a simplification of the ^{13}C spectrum and an increased sensitivity. The most common decoupling sequences are the coherent cyclic decoupling schemes WALTZ-16 [73,74] and MLEV-16 [75–77]. Performance of a specific decoupling scheme depends on the sequence of RF pulses, their shape, duration and amplitude. A detailed review of these decoupling methods can be found elsewhere [78].

The main drawback of broadband decoupling is that it requires a large number of short intense 180° pulses, potentially yielding exceedingly high power deposition in tissues. At high magnetic field, the deposited power already increases in $(B_0)^2$ simply due to

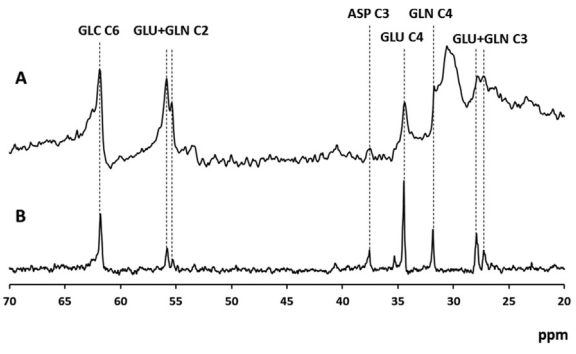

Fig. 4. A) Non-localized ^{13}C Spectra in the rat brain (6-min acquisition). Note the strong lipid contamination around 30 ppm. B) ISIS-DEPT (ISIS-based ^{1}H localization followed by DEPT polarization transfer) in the same animal (20-min acquisition). Experiments were performed at 11.7 T, after ~2-h of [1,6-$^{13}C_2$]glucose infusion.

higher electromagnetic frequency [78]. Furthermore, the decoupling bandwidth must increase linearly if one wants decoupling to be efficient over the same spectral range. This can be achieved by reducing the duration of elementary decoupling pulses as $1/B_0$, in which case the decoupling field amplitude must be increased as B_0, resulting in power deposition increasing as $(B_0)^2$ solely due to the higher decoupling field amplitude [78]. This ultimately results in power deposition increasing more than $(B_0)^2$, actually rather as $(B_0)^2 \times (B_0)^2 = (B_0)^4$. As a consequence, broadband decoupling becomes impractical due to SAR limitations. A low-power broadband stochastic ^{1}H decoupling scheme has been proposed by Li et al. [79] and has been recently applied for ^{13}C MRS studies in Humans at 7 T [40]. This strategy takes advantage of the use of [2-^{13}C]glucose as substrate so as to focus on the detection of the ^{13}C-labeled glutamate, glutamine, GABA, aspartate, and N-acetylaspartate from the carboxylic/amide spectral region (160-185 ppm). Since these carboxylic/amide carbons are coupled *via* significantly weaker ^{13}C-^{1}H scalar couplings ($^2J_{CH} \approx$ 3-5 Hz), less energetic RF pulses can be applied effectively. A "windowed" variant has also been proposed to further decrease the energy deposition by limiting the decoupling to intervals of the ^{1}H spectrum [80].

3.1.5. Chemical shift displacement artefact

Spatial localization of ^{13}C signal is important to minimize contamination from extracranial triacylglycerol resonances and guarantee a certain amount of anatomical specificity. Unfortunately, the large chemical shift dispersion of ^{13}C resonances leads to substantial localization errors. For any resonance of interest, the so-called chemical shift displacement artefact (CSDA) is proportional to the frequency difference with the carrier frequency (which increases with the static magnetic field strength) and inversely proportional to the spectral bandwidth of the spatially selective RF pulse used for slice selection. Since spectral bandwidth are limited by the maximum gradient strength and peak B_1 field intensity available (or allowed by the SAR threshold), CSDA for ^{13}C MRS localization methods are usually much larger than for ^{1}H MRS.

3.1.6. Localized ^{13}C detection

Localization of the ^{13}C signal using ISIS (image selected *in vivo* spectroscopy) or OVS-based localization (using adiabatic pulses with large bandwidth) are valid approaches for *in vivo* ^{13}C MRS studies at moderate magnetic field strength or for narrow chemical shift dispersions. Besides, they can be combined with a nOe presaturation module to achieve up to a 3-fold signal enhancement.

However, it is more advantageous to combine a tridimensional localization scheme of the ^{1}H signal [81,82] with a polarization transfer sequence to minimize the CSDA and achieve up to a four-fold signal enhancement for ^{13}C resonances with relatively long T_2 [83,84].

3.1.7. Polarization transfer

Heteronuclear polarization transfer (PT) experiments offer superior and more consistent signal enhancement than nOe for nuclei with low gyromagnetic ratio J-coupled to ^{1}H nuclei. Through rather complex selective polarization transfer experiments using simultaneous RF pulses on both ^{1}H and ^{13}C spins, PT schemes such as INEPT or DEPT [85,86] manage to drive the ^{13}C polarization to an observable state with an amplitude corresponding to γ_H instead of γ_C, as would result from direct ^{13}C excitation, yielding up to a γ_H/γ_C = 4-fold gain in SNR. Interestingly, the T_1-weighting of the experiment depends on the shorter T_1 relaxation times of the J-coupled protons since the boost of ^{13}C signal originates from the transfer of coherence from the ^{1}H magnetization [87]. Also, TE can be precisely optimized, when knowing ^{13}C-^{1}H scalar coupling constants, to maximize signal enhancement obtained during polarization transfer. An example of DEPT spectrum acquired in the rat brain is shown on Fig. 4B and compared with a non-localized direct ^{13}C spectrum. Another technique to transfer ^{1}H magnetization to ^{13}C magnetization is through Hartmann-Hahn cross-polarization [88]. Optimal cross-polarization transfer is achieved by irradiating both ^{1}H and ^{13}C frequencies during a $1/J_{CH}$ delay with matched B_1 fields on both channel ($\gamma_C B_{1C} = \gamma_H B_{1H}$). For more about polarization transfer, one can read the review by de Graaf et al. [89].

3.2. Indirect ^{1}H-{^{13}C} detection

Even with a 3–4-fold ^{13}C signal enhancement thanks to nOe or polarization transfer, direct ^{13}C MRS suffers from a much lower sensitivity than ^{1}H MRS. In this context, indirect ^{1}H-{^{13}C} MRS is the method of choice when one favors high spatial and/or temporal resolution. In addition, the analysis of ^{1}H spectra allows for an easier access to useful metabolic information such as the pool sizes and the ^{13}C fractional enrichments. However, these ^{1}H-{^{13}C} MRS methods do not benefit from enough spectral resolution to discriminate reliably between many labeling positions, leading to cruder metabolic models.

3.2.1. Broadband ^{13}C decoupling

Broadband ^{13}C decoupling can also be performed for indirect ^{1}H-{^{13}C} acquisition. However, it is complicated by the large chemical shift range of ^{13}C resonances leading to the use of even more energetic RF pulses than for ^{1}H decoupling. Successful use of broadband ^{13}C decoupling in humans have been reported for moderate magnetic field strength ($B_0 \leq 4$ T) [90]. For higher magnetic fields, only preclinical applications have been reported. This suggests that broadband ^{13}C decoupling might not be a viable option for human applications of ^{1}H-{^{13}C} MRS at ultra-high magnetic field.

3.2.2. Heteronuclear spectral editing (POCE & co)

The proton-observed carbon edited method is the most popular ^{1}H-{^{13}C} spectral editing method [91]. With this approach, a 180° inversion pulse is applied every other scan at the ^{13}C frequency at a delay equal to $1/2J_{CH}$ ($\approx$7-8 ms for J_{CH} = 120-150 Hz) before the formation of the ^{1}H echo. When this inversion is On, satellite resonances due to the J-coupling between ^{1}H and ^{13}C nuclei have their phase inverted while resonances from ^{1}H bound to ^{12}C nuclei are unaffected. By subtracting On and Off scans, the signal from ^{1}H bound to ^{13}C nuclei can be observed selectively. POCE can be combined with most ^{1}H localization schemes.

3.2.3. Alternative approaches

As an alternative to editing techniques, we have proposed an approach to detect dynamic ^{13}C labeling without the need of a ^{13}C RF chain. The method is based on the subtraction of ^{1}H spectra, collected during the ^{13}C infusion, from a baseline spectrum acquired prior to infusion [92]. The progressive disappearance of the mother resonance of protons bound to a labeled carbon, replaced by satellites resonances due to heteronuclear coupling, results in a very specific signature on difference spectra, while unlabeled metabolites are suppressed (Fig. 5). We could demonstrate that is was possible to resolve positions C3 and C4 for glutamate during a [U-$^{13}C_6$]glucose infusion in the monkey brain at 3 T. Beyond the easy implementation due to the absence of ^{13}C RF chain, an important advantage of this approach is that it can truly be used with any existing sequence without adaptation (e.g. PRESS [92,93], STEAM [94] and diffusion-weighted STEAM [95]). However, a serious limitation of the technique is that it demands extremely stable acquisition over the entire experiment to avoid subtraction

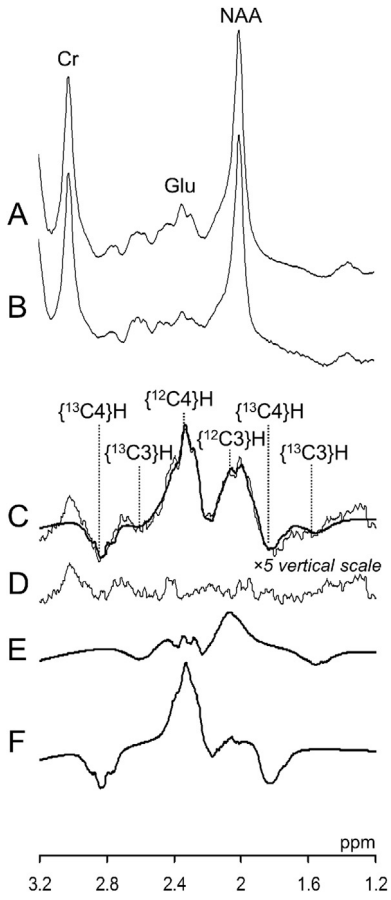

Fig. 5. Strategy to measure ^{13}C labeling without a ^{13}C RF channel, as introduced in Ref. [92]. A) Baseline spectrum acquired at the beginning of an experiment in the monkey brain at 3 T, before the [U-$^{13}C_6$]glucose infusion. B) Spectra collected at the end of the 2-h infusion. C) Difference spectrum (baseline - end of infusion). For Glu C3 and C4, ^{13}C enrichment appears as a typical mother-resonance corresponding to the decrease of the signal of proton bound to ^{12}C, and two negative satellite resonances corresponding to the concomitant increase of protons bound to ^{13}C. The best LCModel fit (see section 3) is also represented. D) Fit residue. E) Contribution of model spectrum accounting for glutamate enriched in position C3. F) Contribution of model spectrum accounting for glutamate enriched in position C4. Note that glutamine was neglected in this analysis.

bias, including shimming and coil sensitivity, as well as total metabolite concentration. Difference spectra are also more complex than POCE spectra, so that advanced spectral analysis is mandatory here (see section 3). Finally, the technique may not work at all magnetic fields, since it behaves poorly when satellite resonances of one group and mother resonance of another group overlap.

3.3. Hardware

With the exception of our alternative method detecting ^{1}H-^{13}C spectral lineshapes [92], the acquisition of ^{13}C NMR spectroscopic data requires several specific elements such as (i) a dual-resonance ^{1}H-^{13}C radiofrequency coil, (ii) ^{1}H and ^{13}C filters and (iii) a broadband amplifier. Also, the NMR Spectrometer must be able to manage two frequencies either simultaneously or with a negligible delay. This last feature is crucial for any polarization transfer or spectral editing sequence and for the use of broadband decoupling. For the sake of simplification, we will consider the set-up for a direct ^{13}C-{^{1}H} MRS experiment (i.e. direct ^{13}C detection with a ^{1}H channel for nOe/PT/decoupling). For an indirect ^{1}H-{^{13}C} MRS experiment, one needs to formally permute the ^{1}H and ^{13}C channels.

3.3.1. Dual-resonance ^{1}H-^{13}C radiofrequency coils

Due to its intrinsically low sensitivity, the ^{13}C RF coil is almost systematically performed using a surface coil instead of a volume coil. Consistently to theoretical analyses in the low-field limit [96], the coil radius is to be adapted to the desired exploration depth ***d*** according to the following formula:

$$r_0 = d/\sqrt{5}. \quad (1)$$

For experiments in rats, this leads to optimal 12-18 mm diameter surface coils depending on the animal head size, whereas for humans studies, much larger 60-90 mm diameters are better suited for optimal sensitivity. The design of the ^{1}H coil is governed by similar rules to optimize its field. However, to limit the crosstalk between both coils, a different geometry for the ^{1}H coil is recommended. The ^{13}C-^{1}H RF coil proposed by Adriany and Gruetter [97] is a popular and efficient design combining a ^{13}C single loop coil with two larger ^{1}H surface coils operating in quadrature (90° phase shift between both loops). As such the ^{1}H quadrature coil allows for a wider yet efficient spatial coverage in particular for decoupling and the acquisition of anatomical images. Alternatively, other quadrature RF coil design such as a “figure 8” or “butterfly” coil has been proposed [98,99] in particular for muscle and cardiac ^{13}C MRS studies.

Recently, Roig et al. [100] have proposed a double-quadrature ^{13}C-^{1}H surface coil enhancing the SNR by nearly $\sqrt{2}$ for the ^{13}C channel compared to the ^{13}C-^{1}H coil proposed by Adriany and Gruetter. To isolate with channels at the proton frequency, proton traps [101] were added to each ^{13}C loop. Using these proton traps is a convenient way to selectively block current induced at the proton frequency while allowing the coil to resonate at the lower frequency [101–103].

Cryogenic RF coil [104] is a very interesting (but costly) technology for detecting low gyromagnetic nuclei such as ^{13}C. Sack et al. [105] have recently demonstrated a greatly enhanced ^{13}C SNR (by a factor of about 4) in the mouse brain at 9.4 T using a ^{13}C Cryoprobe™ (Bruker, Ettlingen, Germany) combined with a saddle ^{1}H coil operating at room temperature. Unfortunately, this technology is only profitable in situations for which thermal noise from the coil dominate sample loss, i.e. for small coils (e.g. for rodents, or small surface coils to study superficial organs in Humans).

For some clinical research application, there are motivations to use dual-resonance volume coils to explore brain metabolism outside of the occipital lobe. A validated design is the double-tuned TEM (transverse electromagnetic) volume coil proposed by Vaughan et al. [106,107]. However, this option comes at a significant cost in terms of sensitivity and RF power efficiency [108]. To alleviate the mutual coupling between coils, B_1 fields can be set orthogonally and traps are necessary [106]. With the exception of very few studies [109], this approach has been limited to indirect ^{1}H-{^{13}C} MRS studies in humans [110,111].

3.3.2. Transmission and reception chains

Despite the limited crosstalk between the ^{1}H and ^{13}C channels (usually around −30 dB), spurious parasitic signals are usually observed during broadband decoupling as a result of significant interferences between RF cables in both transmission and reception chains. Therefore, RF filters are to be set-up at several stages of these transmission and reception chains to achieve a stronger isolation (above −60 dB). Fig. 6 presents a typical setup for a ^{13}C-{^{1}H} MRS experiment. The type, number and positioning of the “^{1}H pass/^{13}C stop” or “^{13}C pass/^{1}H stop” filters may vary according to your NMR spectrometer, the disposition of your cables, or the

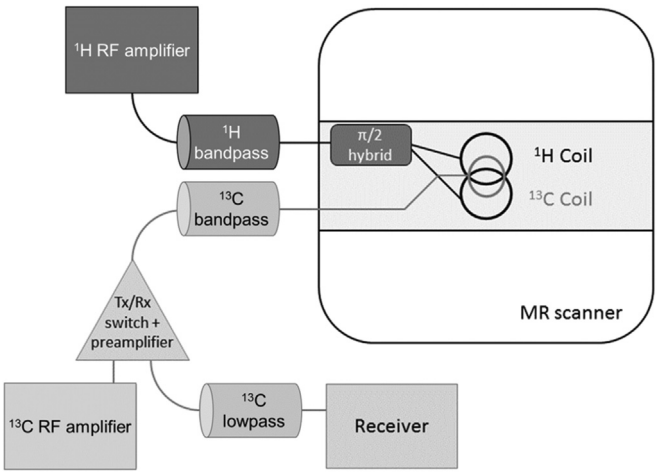

Fig. 6. Typical setup for a direct ^{13}C MRS experiment, with a ^{1}H channel for nOe/polarization transfer/decoupling. Two ^{13}C pass/^{1}H stop filters are positioned before and after the pre-amplification stage to block signal at the ^{1}H frequency. In addition, a ^{1}H pass/^{13}C stop filter is generally placed on the ^{1}H transmission line to minimize subharmonics. For an indirect ^{1}H-{^{13}C} MRS experiment, ^{1}H and ^{13}C should be formally permuted on the picture (and "lowpass" should be replaced by "highpass"). For more details about the setup for indirect ^{1}H-{^{13}C} MRS experiments, one can read the review by de Graaf et al. [89].

decoupling scheme. Regarding the type of RF filters, it is recommended to insert bandpass filters on the transmission line to minimize the harmonic or subharmonic signals generated by the amplifiers. Doing so leads to an insertion loss of about 2 dB which can be detrimental if your peak B_1 field intensity is limited (for example when using volume coils). Low-pass (high-pass for indirect ^{1}H-{^{13}C} detection) filters are usually placed before and after the pre-amplification stage since their insertion loss is lower than 0.5 dB at the ^{13}C NMR frequency.

Finally, it is mandatory that the NMR spectrometer should be equipped with a broadband RF amplifier dedicated for low gyromagnetic nuclei NMR. Unfortunately, this feature is rarely found in MR scanners dedicated to diagnostic de facto limiting ^{13}C (and other low gyromagnetic nuclei) MRS studies to institutions equipped with MR scanner dedicated to clinical research.

4. Quantification of ^{13}C spectra

The quantification of ^{13}C spectra, i.e. the determination of the fractional enrichment (in percent) or absolute concentration (in mM or µmol/g) of ^{13}C-labeled metabolites, can be considered as the outcome of ^{13}C experiments, or the last step before performing metabolic modeling.

Quantification can be achieved at the positional level with direct or indirect detection, i.e. the amount of ^{13}C at a given atomic position is quantified irrespective of the labeling at other atomic positions. In direct detection, quantification can also be achieved at the isotopomer level, which in theory provides more information than the sole positional enrichments [41,112]. However, since isotopomer detection relies on scalar ^{13}C-^{13}C scalar J-coupling, it is possible only if the linewidth is narrower than J-coupling constant (which is not possible with poor shim, or at very high magnetic field). Note that isotopomers, i.e. the different labeling combinations for individual molecules, are actually not directly detected on spectra, and cannot all be determined from spectral analysis. This is rather the fine multiplet structure, which depends on the labeling of immediate neighbors, which is quantified on spectra: singlets, corresponding to unlabeled neighbors; doublets, corresponding to only one labeled neighbor; and triplets and quadruplets, corresponding to two labeled neighbors, respectively with identical or different J-coupling constants. This fine structure can then be connected to bonded cumomers, which represent some classes of isotopomers accessible to ^{13}C MRS (see Ref. [41] for a detailed explanation of the concept of bonded cumomer and the relation with multiplet structure, and [112,113] for *in vivo* applications). In any case, this crucial step requires much attention to minimize quantification bias.

4.1. Measuring metabolite signal

Measuring the amount of signal for each resonance, in some arbitrary unit, is a prerequisite for any quantification of ^{13}C labeling. In early days this was achieved by measuring peak height, or peak area. The latter is more accurate, because it accounts for line-broadening due to T_2. However, peaks must be well separated, which is the case only for well shimmed direct ^{13}C spectra, or at very high magnetic fields for indirect ^{13}C MRS (and even in that case, some resonances will still overlap on indirect spectra, such as glutamate and glutamine C3). To overcome this limitation, spectral fitting using linear combination of individual metabolite spectra (e.g. with commercially available software LCModel [114]) has been used to quantify signal at different atomic positions on indirect spectra, or even on baseline-infusion subtraction spectra (Fig. 5). Each spectrum of the basis-set used for the linear analysis represents the signal of a metabolite enriched at a single atomic position, as obtained with the MRS sequence used, which can advantageously be generated by density matrix simulation to take coupling effects into account (in particular, see Ref. [115] for the importance of accounting for strong coupling, which results in signal "bleeding" from labeled atomic positions to unlabeled ones on POCE spectra). LCModel has also been proposed to quantify ^{13}C spectra *in vivo* [116], which proved very powerful to quantify the different ^{13}C fine spectral structures corresponding to isotopomers (i.e. separately quantify singlets, doublet, triplets and quadruplets at a given atomic position, see Fig. 7). It was also shown that LCModel allowed overcoming the increased spectral complexity in non-decoupled ^{13}C spectra acquired in the brain during [1,6-$^{13}C_2$]glucose infusion [117], demonstrating that advanced analysis tools can somehow alleviate the need for heteronuclear decoupling. When used on direct spectra, LCModel must be configured specifically to cope

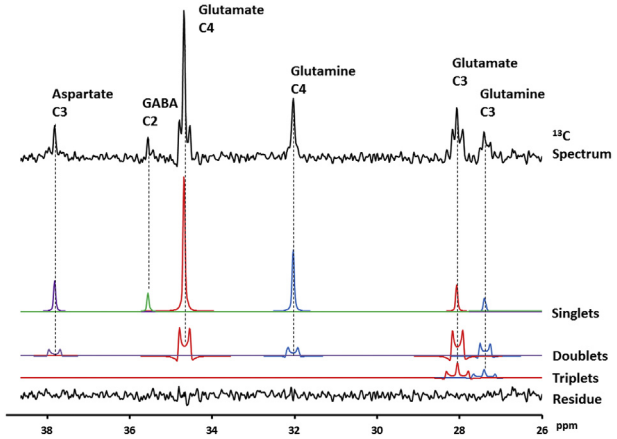

Fig. 7. Linear combination analysis by LCModel of a ^{13}C spectrum acquired in the rat brain at 11.7 T during an infusion of [1,6-$^{13}C_2$]glucose using an ISIS-DEPT sequence. Spectrum was acquired ~100 min after the start of the infusion, for a total acquisition time of 20 min.

with features of ^{13}C spectra, e.g. the very large spectral width (more details about LCModel configuration can be found in Ref. [116]). We also refer the reader to [116] to find ^{13}C chemical shifts and homonuclear J-coupling values as measured *in vivo*, which can be useful to generate the adequate individual spectra for the basis-set. More recently, freely available software AMARES [118] has been used as an efficient alternative to LCModel for isotopomer quantification, as exhaustively described in Ref. [119]. Whatever the method used, at the end of the procedure the signal has been quantified in arbitrary units, which need to be converted to fractional enrichment and absolute ^{13}C concentration. The situation is very different for direct and indirect ^{13}C MRS, as explained below.

4.2. Conversion of signal amplitude to FE and absolute concentrations in indirect detection

Indirect detection allows relatively straightforward quantification, because the total signal ($^{12}C+^{13}C$) for a given metabolite can be measured on an unedited ^{1}H spectrum in the same arbitrary unit as the signal of the labeled fraction for this metabolite, provided both the edited and unedited spectra are acquired with the same sequence (e.g. all the unedited scans for a POCE sequence). The FE is then directly determined by calculating signal ratio. Note that, if editing is not perfect (e.g. imperfect inversion pulses on the ^{13}C channel), the signal on the edited spectrum will be lower, leading to underestimation of FE. This bias can be avoided if adiabatic inversion is used.

Generally speaking, calculating the absolute concentration of metabolites relies on some signal calibration, to convert arbitrary signal units to mM (or μmol/g) [120]. This usually requires an internal reference of known concentration, such as water, which in indirect MRS can advantageously be measured with the same sensitivity as the metabolites (i.e. using the same unedited sequence, same RF coils, same acquisition gain etc…). The ratio of metabolite signal *versus* water signal can then be used to determine metabolite concentration, since water concentration can be estimated after tissue segmentation in the voxel, knowing water concentration in each tissue type. T_1 and T_2 relaxation may be taken into account to correct for signal ratio and yield more accurate results, in particular for short TR/long TE experiments, but this requires knowing relaxation times for water and metabolites. Finally, once metabolite total concentration is known, going from FE to absolute ^{13}C concentration is straightforward.

4.3. Conversion of signal amplitude to FE and absolute concentrations in direct detection

Signal quantification in direct detection remains simple if an indirect experiment can be performed *in vivo*, in addition to the direct experiment. For example, let's assume that the labeling kinetics are measured by direct ^{13}C MRS, and that an indirect measurement is performed at the end of the infusion to determine metabolite FE and absolute ^{13}C concentration (see 3.2). The ^{13}C labeling time-curves can then be converted to mM by scaling them with the absolute ^{13}C concentrations estimated at the end of the curves. When possible in a preclinical context, animals may also be sacrificed at the end of the perfusion to perform high-resolution indirect MRS of brain extracts to determine FE and metabolite concentration, allowing subsequent scaling of *in vivo* ^{13}C time-curves. However in this latter case, one must be wary that FE and metabolite concentrations derived from *ex vivo* tissue extracts may not reflect *in vivo* ones, simply because extracted tissues may not exactly represent the tissue content of the voxel (to say nothing of the possible variation in metabolite content after sacrifice).

If indirect detection is not possible, determination of FE can sometimes be achieved in direct detection in a quite simple way using isotopomer analysis, provided fine multiplet structures can be individually quantified and labeling at neighbor atomic positions occurs randomly, as detailed in Ref. [116]. For example, determining the fractional enrichment of glutamate at position C3 during an infusion [1-^{13}C] or [1,6-$^{13}C_2$]glucose can be achieved by calculating signal ratio of the C4 doublet (C4D43) relative to the total C4 signal, i.e. the sum of the singlet C4S and of the doublet C4D43 (provided C5 is not labeled, which would made impossible to distinguish between C4D43 and C4D45). However, this elegant method requires all multiplet structures to be reliably quantified, which might prove difficult in most situations.

If FE could be determined using one of the approach described above, ^{13}C concentrations are then simply given by these FE multiplied by metabolite absolute concentrations, as tabulated or determined on ^{1}H spectra [120]. If FE cannot be determined, one will need to quantify ^{13}C absolute concentration on ^{13}C spectra, using again some signal calibration. Two difficulties regarding calibration are particularly salient for direct detection compared to indirect detection. First, it is difficult to find a reliable ^{13}C reference of known concentration. An external reference (positioned within the detection region of the coil) can be used, but correcting for the different sensitivities between the *in vivo* voxel and the phantom, due to inhomogeneous transmit and receive B_1 fields, will require careful calibration and validation steps. Signal calibration can also be achieved before *in vivo* experiments, by doing experiments on a phantom with known ^{13}C concentration positioned exactly like the organ of interest, and assuming that coil loading and sensitivity will be exactly identical *in vivo* [121]. Using an internal reference allows avoiding these potential sources of bias, but there is no easily accessible internal reference. If detection sensitivity is good enough, some natural abundance signal might be quantified (even if this requires averaging all spectra acquired during the ^{13}C-infusion). A good candidate can be myo-inositol or NAA at position C6 [11], which is only very slowly labeled.

Second, the excitation profile will usually not be homogeneous throughout the spectral region of interest, especially at high fields where the frequency dispersion is increased. This is due to the non-flat profile of radiofrequency pulses due to the very broad chemical shift dispersion of ^{13}C resonances, but also to the variable efficiency of nOe or polarization transfer. The signal ratio between the metabolites and the reference (possibly a resonance of an observed metabolite) must therefore be corrected by the excitation profile to determine the absolute concentration of ^{13}C-labeled metabolites. This can be calibrated on a phantom containing metabolites of interest, with known concentrations (even at natural abundance), however calibration errors due to differences in relaxation times between phantom and *in vivo* conditions may arise.

An important practical situation is when FE can be determined, but only for a single prominent resonance of the spectrum, e.g. in an indirect experiment performed with a suboptimal coil setup (optimized for direct ^{13}C detection), or by isotopomer analysis on this resonance. It can then be used to determine FE for other atomic positions and other metabolites on direct spectra, using the calibration on metabolite phantom as described above. Using this approach, it is really desirable to determine FE at least for one atomic position of each metabolite, and then work on a metabolite-per-metabolite basis, in order to mitigate possible bias due to metabolite-specific variations in relaxation times between *in vivo* and phantom conditions: for example, determine FE for glutamate C3 based on isotopomer analysis, and from here determine FE for other atomic positions of glutamate by signal ratio (taking into account the calibration factors determined on phantom); then, repeat exactly the same procedure for other metabolites. Such a

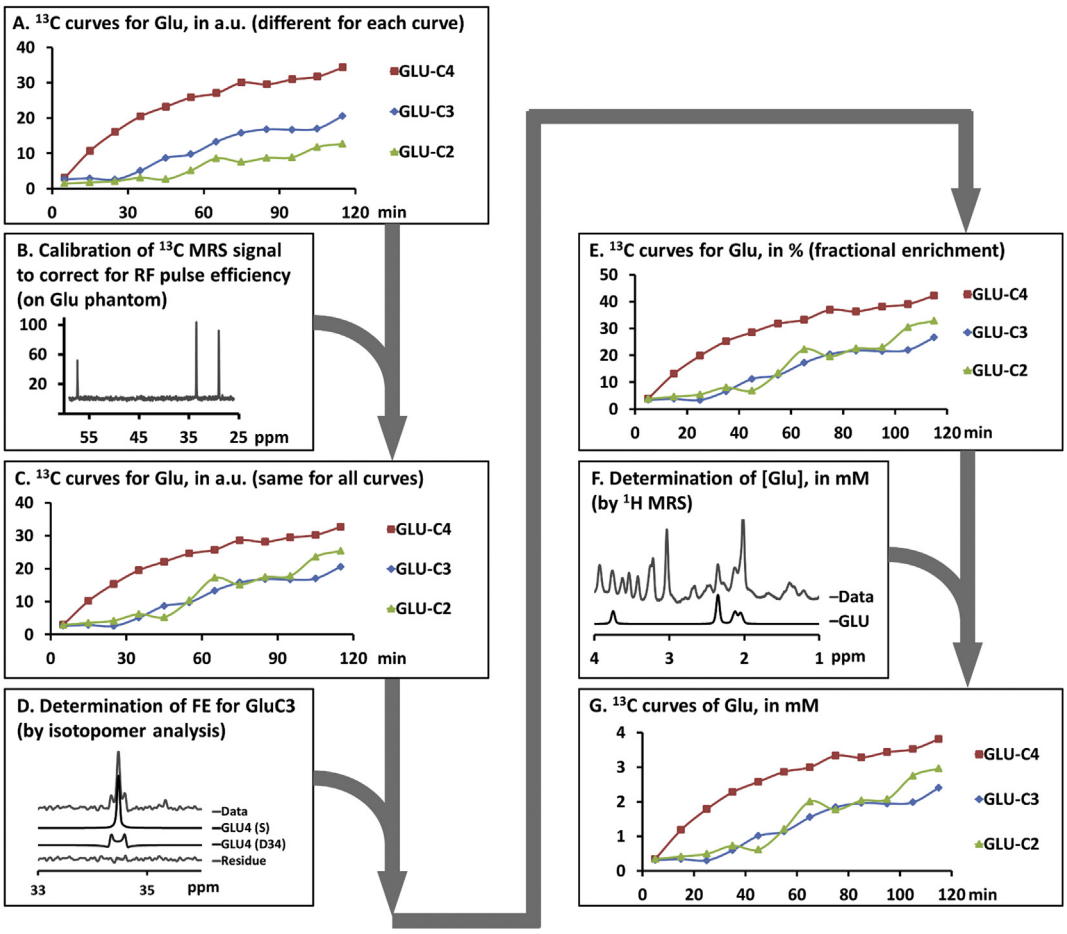

Fig. 8. Workflow for the absolute quantification of ^{13}C time curves, in mM, in one of the situation described in the main text, when no internal reference is available, and FE can be determined only for a single prominent resonance of the spectrum. (A) After spectral analysis (e.g. using LCModel), ^{13}C labeling curves are obtained for glutamate at position C2, C3 and C4, in arbitrary units. The signal amplitude of different atomic positions as determined on a glutamate phantom (B) is used to correct for the non-uniform excitation profile of the sequence and rescale the *in vivo* labeling curves in the same arbitrary units (C). In (D), the FE of a glutamate C3 is determined, here using isotopomer analysis on glutamate C4: FE(C3) = C4D43/(C4S + C4D43). Since glutamate labeling curves are already in the same arbitrary units, this allows direct scaling of all curves to FE (E). Glutamate concentration (in mM), as determined by ^{1}H MRS *in vivo* before the infusion (F), is finally used to convert FE in mM (G).

procedure is represented on Fig. 8.

5. Perspectives

In this review we have provided some keys to understand and design ^{13}C MRS experiments, from the infusion protocol to the spectral quantification. We hope that we have convinced the readers that great care should be taken at all stages, and that they will find some help in these pages to design their experiments and derive meaningful ^{13}C enrichments with respect to the metabolic question asked. We have not addressed metabolic modeling, which goes beyond the "experimental" aspects described here, and for more information about metabolic modeling we refer the readers to the numerous papers devoted to this topic (e.g. see Ref. [122] for detailed derivation of the bi-compartmental neuron-astrocyte model in the brain, [123] for didactic presentation of model generation and utilization, and [112] for isotopomer modeling and possible refinements of the bi-compartmental model).

What are the perspectives for ^{13}C MRS, as NMR technology keeps improving? It is quite general to say that increased magnetic field will lead to increased sensitivity. This seems to be the case for ^{13}C at first sight, because ^{13}C frequency remains relatively low, even at very high fields (~121 MHz at 11.7 T), so that B_1 homogeneity issues arising at ultra-high frequencies when the investigated object is not small compared to wavelength (e.g. in the Human brain for ^{1}H at 7 T or higher) should be avoided. However, this statement should be carefully nuanced, in particular in Humans. Indeed, indirect ^{13}C detection and polarization transfer requires 90° or 180° flips at ^{1}H frequencies, so that B_1 homogeneity issues remain critical, unless direct ^{13}C excitation and detection is used. However, in direct ^{13}C excitation, CSDA will become rapidly unmanageable at high fields. And in all cases, broadband decoupling will remain extremely challenging in terms of SAR (although the use of spectral analysis tools such as LCModel may alleviate the need for decoupling [117], but at the expense of SNR). In this context, it is unclear that increased magnetic field can compensate for the decreased sensitivity resulting from abandoning indirect detection, polarization transfer and decoupling. This emphasizes how ^{13}C MRS in Humans at high fields will benefit from methodological progresses in ultra-high frequency MRI, in particular parallel transmission and RF pulse design. Another possible limitation to ^{13}C MRS at very high fields might be that, as the linewidth is increasing and therefore becoming not negligible compared to J-coupling constant, the quantification of multiplet fine structure and corresponding isotopomer analysis is getting more difficult.

Beyond the magnetic field, SNR can be increased by improving the sensitivity of RF coils. This will in general be much cheaper than increasing the magnetic field, and will not raise the problems

associated with ultra-high frequencies, as mentioned above. Over the past years, cryogenic coils have been introduced for *in vivo* use in the rodent brain, yielding ~2-fold sensitivity gains in ^{1}H detection. The gain is expected to be even better at the lower ^{13}C frequency. As already mentioned in section 2, we are aware of one ^{13}C cryogenic coil developed for the mouse brain, yielding up to 4-fold sensitivity gain at 9.4 T [105]. However, we think that the current design for ^{13}C cryogenic coil is still in its infancy: in particular, an efficient ^{1}H transmission coil needs to be combined with the ^{13}C cryogenic coil to yield ^{1}H pulses with high B_1, for polarization transfer and broadband decoupling. Reciprocally, for indirect detection, ^{1}H cryogenic probes should be combined with efficient ^{13}C transmission coils, which as far as we know has not been achieved yet. In our opinion, the successful realization of any of these two different coil setups could represent a major breakthrough for ^{13}C MRS in rodents.

We could not conclude without a word about hyperpolarization, although this is not the topic of the present paper. ^{13}C hyperpolarization can in theory increase SNR by a factor up to ~10^5, opening fantastic possibilities described elsewhere in this journal special issue, in particular for tumor imaging [124–126]. However, hyperpolarization is obviously not a general method to enhance sensitivity, since hyperpolarization is not performed on endogenous metabolites *in vivo*, but on a limited number of ^{13}C-labeled substrates which then need to be injected. Moreover, hyperpolarized magnetization relaxes towards its thermal equilibrium value according to T1 relaxation time (typical T1 for hyperpolarized substrates, such as [1-^{13}C]pyruvate, [2-^{13}C]pyruvate or [1-^{13}C]αKG, range from 20 to 60 s, depending on the field [127]). This leaves relatively little time to label compounds lying far downstream on metabolic pathways, or derived from substrates *via* very slow biochemical reactions, so that only a limited number of metabolic fluxes are accessible to hyperpolarization.

References

[1] D.L. Rothman, H.M. De Feyter, R.A. de Graaf, G.F. Mason, K.L. Behar, 13C MRS studies of neuroenergetics and neurotransmitter cycling in humans, NMR Biomed. 24 (8) (2011) 943–957.

[2] T.B. Rodrigues, J. Valette, A.K. Bouzier-Sore, (13)C NMR spectroscopy applications to brain energy metabolism, Front. Neuroenergetics 5 (2013) 9.

[3] E.L. Thomas, J.D. Hanrahan, M. Ala-Korpela, G. Jenkinson, D. Azzopardi, R.A. Iles, J.D. Bell, Noninvasive characterization of neonatal adipose tissue by 13C magnetic resonance spectroscopy, Lipids 32 (6) (1997) 645–651.

[4] J.H. Hwang, S. Bluml, A. Leaf, B.D. Ross, In vivo characterization of fatty acids in human adipose tissue using natural abundance 1H decoupled 13C MRS at 1.5 T: clinical applications to dietary therapy, NMR Biomed. 16 (3) (2003) 160–167.

[5] R. Gruetter, T.A. Prolla, R.G. Shulman, 13C NMR visibility of rabbit muscle glycogen in vivo, Magn. Reson. Med. 20 (2) (1991) 327–332.

[6] R. Taylor, T.B. Price, D.L. Rothman, R.G. Shulman, G.I. Shulman, Validation of 13C NMR measurement of human skeletal muscle glycogen by direct biochemical assay of needle biopsy samples, Magn. Reson. Med. 27 (1) (1992) 13–20.

[7] R. Gruetter, I. Magnusson, D.L. Rothman, M.J. Avison, R.G. Shulman, G.I. Shulman, Validation of 13C NMR measurements of liver glycogen in vivo, Magn. Reson. Med. 31 (6) (1994) 583–588.

[8] T.B. Price, Regulation of glycogen metabolism in muscle during exercise, in: R.G. Shulman, D.L. Rothman (Eds.), Metabolomics by in Vivo NMR, John Wiley & Sons, Ltd, 2004.

[9] G.F. Mason, K.F. Petersen, R.A. de Graaf, T. Kanamatsu, T. Otsuki, D.L. Rothman, A comparison of C-13 NMR measurements of the rates of glutamine synthesis and the tricarboxylic acid cycle during oral and intravenous administration of [1-C-13]glucose (vol 10, pg 181, 2003), Brain Res. Protoc. 11 (2) (2003), 143–143.

[10] B. Ross, A. Lin, K. Harris, P. Bhattacharya, B. Schweinsburg, Clinical experience with 13C MRS in vivo, NMR Biomed. 16 (6–7) (2003) 358–369.

[11] F. Boumezbeur, K.F. Petersen, G.W. Cline, G.F. Mason, K.L. Behar, G.I. Shulman, D.L. Rothman, The contribution of blood lactate to brain energy metabolism in humans measured by dynamic C-13 nuclear magnetic resonance spectroscopy, J. Neurosci. 30 (42) (2010) 13983–13991.

[12] S.M. Cohen, R.G. Shulman, A.C. McLaughlin, Effects of ethanol on alanine metabolism in perfused mouse liver studied by 13C NMR, Proc. Natl. Acad. Sci. U. S. A. 76 (10) (1979) 4808–4812.

[13] C. Pahl-Wostl, J. Seelig, Metabolic pathways for ketone body production. 13C NMR spectroscopy of rat liver in vivo using 13C-multilabeled fatty acids, Biochemistry 25 (22) (1986) 6799–6807.

[14] E.S. Jin, A.D. Sherry, C.R. Malloy, Metabolism of glycerol, glucose, and lactate in the citric acid cycle prior to incorporation into hepatic acylglycerols, J. Biol. Chem. 288 (20) (2013) 14488–14496.

[15] I.A. Bailey, D.G. Gadian, P.M. Matthews, G.K. Radda, P.J. Seeley, Studies of metabolism in the isolated, perfused rat-heart using C-13 Nmr, FEBS Lett. 123 (2) (1981) 315–318.

[16] A.D. Sherry, R.L. Nunnally, R.M. Peshock, Metabolic studies of pyruvate- and lactate-perfused guinea pig hearts by 13C NMR. Determination of substrate preference by glutamate isotopomer distribution, J. Biol. Chem. 260 (16) (1985) 9272–9279.

[17] A.D. Sherry, C.R. Malloy, R.E. Roby, A. Rajagopal, F.M. Jeffrey, Propionate metabolism in the rat heart by 13C n.m.r. spectroscopy, Biochem. J. 254 (2) (1988) 593–598.

[18] E.S. Jin, A.D. Sherry, C.R. Malloy, Lactate contributes to glyceroneogenesis and glyconeogenesis in skeletal muscle by reversal of pyruvate kinase, J. Biol. Chem. 290 (51) (2015) 30486–30497.

[19] S. Cerdan, B. Kunnecke, J. Seelig, Cerebral metabolism of [1,2-13C2]acetate as detected by in vivo and in vitro 13C NMR, J. Biol. Chem. 265 (22) (1990) 12916–12926.

[20] V. Lebon, K.F. Petersen, G.W. Cline, J. Shen, G.F. Mason, S. Dufour, K.L. Behar, G.I. Shulman, D.L. Rothman, Astroglial contribution to brain energy metabolism in humans revealed by 13C nuclear magnetic resonance spectroscopy: elucidation of the dominant pathway for neurotransmitter glutamate repletion and measurement of astrocytic oxidative metabolism, J. Neurosci. 22 (5) (2002) 1523–1531.

[21] F. Boumezbeur, G.F. Mason, R.A. de Graaf, K.L. Behar, G.W. Cline, G.I. Shulman, D.L. Rothman, K.F. Petersen, Altered brain mitochondrial metabolism in healthy aging as assessed by in vivo magnetic resonance spectroscopy, J. Cereb. Blood Flow Metab. 30 (1) (2010) 211–221.

[22] B. Kunnecke, S. Cerdan, J. Seelig, Cerebral metabolism of [1,2-13C2]glucose and [U-13C4]3-hydroxybutyrate in rat brain as detected by 13C NMR spectroscopy, NMR Biomed. 6 (4) (1993) 264–277.

[23] S.V. Gonzalez, N.H. Nguyen, F. Rise, B. Hassel, Brain metabolism of exogenous pyruvate, J. Neurochem. 95 (1) (2005) 284–293.

[24] A.K. Bouzier, E. Thiaudiere, M. Biran, R. Rouland, P. Canioni, M. Merle, The metabolism of [3-C-13]lactate in the rat brain is specific of a pyruvate carboxylase-deprived compartment, J. Neurochem. 75 (2) (2000) 480–486.

[25] J.M.N. Duarte, F.M. Girault, R. Gruetter, Brain energy metabolism measured by C-13 magnetic resonance spectroscopy in vivo upon infusion of [3-C-13] lactate, J. Neurosci. Res. 93 (7) (2015) 1009–1018.

[26] P. Bagga, K.L. Behar, G.F. Mason, H.M. De Feyter, D.L. Rothman, A.B. Patel, Characterization of cerebral glutamine uptake from blood in the mouse brain: implications for metabolic modeling of 13C NMR data, J. Cereb. Blood Flow Metab. 34 (10) (2014) 1666–1672.

[27] J.R. Alger, L.O. Sillerud, K.L. Behar, R.J. Gillies, R.G. Shulman, R.E. Gordon, D. Shae, P.E. Hanley, In vivo carbon-13 nuclear magnetic resonance studies of mammals, Science 214 (4521) (1981) 660–662.

[28] K.F. Petersen, D. Laurent, D.L. Rothman, G.W. Cline, G.I. Shulman, Mechanism by which glucose and insulin inhibit net hepatic glycogenolysis in humans, J. Clin. InvestInvestig. 101 (6) (1998) 1203–1209.

[29] I.Y. Choi, I. Tkac, K. Ugurbil, R. Gruetter, Noninvasive measurements of [1-(13)C]glycogen concentrations and metabolism in rat brain in vivo, J. Neurochem. 73 (3) (1999) 1300–1308.

[30] G. Oz, E.R. Seaquist, A. Kumar, A.B. Criego, L.E. Benedict, J.P. Rao, P.G. Henry, P.F. Van De Moortele, R. Gruetter, Human brain glycogen content and metabolism: implications on its role in brain energy metabolism, Am. J. Physiol. Endocrinol. Metab. 292 (3) (2007) E946–E951.

[31] F.D. Morgenthaler, R.B. van Heeswijk, L.J. Xin, S. Laus, H. Frenkel, H.X. Lei, R. Gruetter, Non-invasive quantification of brain glycogen absolute concentration, J. Neurochem. 107 (5) (2008) 1414–1423.

[32] F.D. Morgenthaler, B.R. Lanz, J.M. Petit, H. Frenkel, P.J. Magistretti, R. Gruetter, Alteration of brain glycogen turnover in the conscious rat after 5h of prolonged wakefulness, Neurochem. Int. 55 (1–3) (2009) 45–51.

[33] R.B. van Heeswijk, F.D. Morgenthaler, L.J. Xin, R. Gruetter, Quantification of brain glycogen concentration and turnover through localized C-13 NMR of both the C1 and C6 resonances, NMR Biomed. 23 (3) (2010) 270–276.

[34] N. Tesfaye, E.R. Seaquist, G. Oz, Noninvasive measurement of brain glycogen by nuclear magnetic resonance spectroscopy and its application to the study of brain metabolism, J. Neurosci. Res. 89 (12) (2011) 1905–1912.

[35] A. Khowaja, I.Y. Choi, E.R. Seaquist, G. Oz, In vivo Magnetic Resonance Spectroscopy of cerebral glycogen metabolism in animals and humans, Metab. Brain Dis. 30 (1) (2015) 255–261.

[36] E.M. Chance, S.H. Seeholzer, K. Kobayashi, J.R. Williamson, Mathematical analysis of isotope labeling in the citric acid cycle with applications to 13C NMR studies in perfused rat hearts, J. Biol. Chem. 258 (22) (1983) 13785–13794.

[37] G.F. Mason, D.L. Rothman, K.L. Behar, R.G. Shulman, NMR determination of the TCA cycle rate and alpha-ketoglutarate/glutamate exchange rate in rat brain, J. Cereb. Blood Flow Metab. 12 (3) (1992) 434–447.

[38] A. Ziegler, C.E. Zaugg, P.T. Buser, J. Seelig, B. Kunnecke, Non-invasive measurements of myocardial carbon metabolism using in vivo 13C NMR spectroscopy, NMR Biomed. 15 (3) (2002) 222–234.

[39] D.E. Befroy, R.J. Perry, N. Jain, S. Dufour, G.W. Cline, J.K. Trimmer, J. Brosnan, D.L. Rothman, K.F. Petersen, G.I. Shulman, Direct assessment of hepatic mitochondrial oxidative and anaplerotic fluxes in humans using dynamic 13C magnetic resonance spectroscopy, Nat. Med. 20 (1) (2014) 98–102.
[40] S. Li, L. An, S. Yu, M. Ferraris Araneta, C.S. Johnson, S. Wang, J. Shen, (13) C MRS of human brain at 7 Tesla using [2-(13) C]glucose infusion and low power broadband stochastic proton decoupling, Magn. Reson. Med. 75 (3) (2016) 954–961.
[41] A.A. Shestov, J. Valette, D.K. Deelchand, K. Ugurbil, P.G. Henry, Metabolic modeling of dynamic brain (1)(3)C NMR multiplet data: concepts and simulations with a two-compartment neuronal-glial model, Neurochem. Res. 37 (11) (2012) 2388–2401.
[42] R.A. Waniewski, D.L. Martin, Preferential utilization of acetate by astrocytes is attributable to transport, J. Neurosci. 18 (14) (1998) 5225–5233.
[43] D.K. Deelchand, C. Nelson, A.A. Shestov, K. Ugurbil, P.G. Henry, Simultaneous measurement of neuronal and glial metabolism in rat brain in vivo using co-infusion of [1,6-C-13(2)]glucose and [1,2-C-13(2)]acetate, J. Magn. Reson. 196 (2) (2009) 157–163.
[44] N.R. Sibson, G.F. Mason, J. Shen, G.W. Cline, A.Z. Herskovits, J.E.M. Wall, K.L. Behar, D.L. Rothman, R.G. Shulman, In vivo C-13 NMR measurement of neurotransmitter glutamate cycling, anaplerosis and TCA cycle flux in rat brain during [2-C-13]glucose infusion, J. Neurochem. 76 (4) (2001) 975–989.
[45] G.F. Mason, K.F. Petersen, R.A. de Graaf, G.I. Shulman, D.L. Rothman, Measurements of the anaplerotic rate in the human cerebral cortex using 13C magnetic resonance spectroscopy and [1-13C] and [2-13C] glucose, J. Neurochem. 100 (1) (2007) 73–86.
[46] O.A. Petroff, L.D. Errante, D.L. Rothman, J.H. Kim, D.D. Spencer, Glutamate-glutamine cycling in the epileptic human hippocampus, Epilepsia 43 (7) (2002) 703–710.
[47] I.Y. Choi, H. Lei, R. Gruetter, Effect of deep pentobarbital anesthesia on neurotransmitter metabolism in vivo: on the correlation of total glucose consumption with glutamatergic action, J. Cereb. Blood Flow Metab. 22 (11) (2002) 1343–1351.
[48] N.R. Sibson, A. Dhankhar, G.F. Mason, D.L. Rothman, K.L. Behar, R.G. Shulman, Stoichiometric coupling of brain glucose metabolism and glutamatergic neuronal activity, Proc. Natl. Acad. Sci. U. S. A. 95 (1) (1998) 316–321.
[49] A.B. Patel, R.A. de Graaf, G.F. Mason, T. Kanamatsu, D.L. Rothman, R.G. Shulman, K.L. Behar, Glutamatergic neurotransmission and neuronal glucose oxidation are coupled during intense neuronal activation, J. Cereb. Blood Flow Metab. 24 (9) (2004) 972–985.
[50] J. Yang, C.Q. Li, J. Shen, In vivo detection of cortical GABA turnover from intravenously infused [1-13C]D-glucose, Magn. Reson. Med. 53 (6) (2005) 1258–1267.
[51] J. Shen, D.L. Rothman, K.L. Behar, S. Xu, Determination of the glutamate-glutamine cycling flux using two-compartment dynamic metabolic modeling is sensitive to astroglial dilution, J. Cereb. Blood Flow Metab. 29 (1) (2009) 108–118.
[52] N. Auestad, R.A. Korsak, J.W. Morrow, J. Edmond, Fatty acid oxidation and ketogenesis by astrocytes in primary culture, J. Neurochem. 56 (4) (1991) 1376–1386.
[53] D. Ebert, R.G. Haller, M.E. Walton, Energy contribution of octanoate to intact rat brain metabolism measured by 13C nuclear magnetic resonance spectroscopy, J. Neurosci. 23 (13) (2003) 5928–5935.
[54] B. Lanz, L. Xin, P. Millet, R. Gruetter, In vivo quantification of neuro-glial metabolism and glial glutamate concentration using 1H-[13C] MRS at 14.1T, J. Neurochem. 128 (1) (2014) 125–139.
[55] A.B. Patel, R.A. de Graaf, G.F. Mason, D.L. Rothman, R.G. Shulman, K.L. Behar, The contribution of GABA to glutamate/glutamine cycling and energy metabolism in the rat cortex in vivo, Proc. Natl. Acad. Sci. U. S. A. 102 (15) (2005) 5588–5593.
[56] A.B. Patel, R.A. de Graaf, D.L. Rothman, K.L. Behar, Effects of gamma-Aminobutyric acid transporter 1 inhibition by tiagabine on brain glutamate and gamma-Aminobutyric acid metabolism in the anesthetized rat in vivo, J. Neurosci. Res. 93 (7) (2015) 1101–1108.
[57] J. Yang, S.Z.S. Li, J. Bacher, J. Shen, Quantification of cortical GABA-glutamine cycling rate using in vivo magnetic resonance signal of [2-C-13]GABA derived from glia-specific substrate [2-C-13]acetate, Neurochem. Int. 50 (2) (2007) 371–378.
[58] F. Boumezbeur, K.F. Petersen, G.I. Shulman, D.L. Rothman, G.F. Mason, Measurement of the GABA/Glutamine cycling rate in the human brain using 13C MRS, Proc. Int. Soc. Mag. Reson Med. (2007) 15.
[59] P. van Eijsden, K.L. Behar, G.F. Mason, K.P. Braun, R.A. de Graaf, In vivo neurochemical profiling of rat brain by 1H-[13C] NMR spectroscopy: cerebral energetics and glutamatergic/GABAergic neurotransmission, J. Neurochem. 112 (1) (2010) 24–33.
[60] R. Gruetter, G. Adriany, I.Y. Choi, P.G. Henry, H. Lei, G. Oz, Localized in vivo 13C NMR spectroscopy of the brain, NMR Biomed. 16 (6–7) (2003) 313–338.
[61] D.I. Hoult, R.E. Richards, The signal-to-noise ratio of nuclear magnetic resonance experiment, J. Magn. Reson. 24 (1976) 71–85.
[62] A.J. van den Bergh, H.J. van den Boogert, A. Heerschap, Skin temperature increase during local exposure to high-power RF levels in humans, Magn. Reson. Med. 43 (3) (2000) 488–490.
[63] A.J. van den Bergh, H.J. van den Boogert, A. Heerschap, Calibration of the 1H decoupling field strength and experimental evaluation of the specific RF absorption rate in 1H-decoupled human 13C-MRS, Magn. Reson. Med. 39 (4) (1998) 642–646.
[64] I.Y. Choi, I. Tkac, R. Gruetter, Single-shot, three-dimensional "non-echo" localization method for in vivo NMR spectroscopy, Magn. Reson. Med. 44 (3) (2000) 387–394.
[65] T.B. Price, D.L. Rothman, R.G. Shulman, NMR of glycogen in exercise, Proc. Nutr. Soc. 58 (4) (1999) 851–859.
[66] V. Lebon, S. Dufour, K.F. Petersen, J. Ren, B.M. Jucker, L.A. Slezak, G.W. Cline, D.L. Rothman, G.I. Shulman, Effect of triiodothyronine on mitochondrial energy coupling in human skeletal muscle, J. Clin. Invest 108 (5) (2001) 733–737.
[67] J.J. Prompers, J.A. Jeneson, M.R. Drost, C.C. Oomens, G.J. Strijkers, K. Nicolay, Dynamic MRS and MRI of skeletal muscle function and biomechanics, NMR Biomed. 19 (7) (2006) 927–953.
[68] D.E. Befroy, K. Falk Petersen, D.L. Rothman, G.I. Shulman, Assessment of in vivo mitochondrial metabolism by magnetic resonance spectroscopy, Methods Enzym. 457 (2009) 373–393.
[69] I.Y. Choi, R. Gruetter, In vivo 13C NMR assessment of brain glycogen concentration and turnover in the awake rat, Neurochem. Int. 43 (4–5) (2003) 317–322.
[70] I.Y. Choi, E.R. Seaquist, R. Gruetter, Effect of hypoglycemia on brain glycogen metabolism in vivo, J. Neurosci. Res. 72 (1) (2003) 25–32.
[71] G. Oz, P.G. Henry, E.R. Seaquist, R. Gruetter, Direct, noninvasive measurement of brain glycogen metabolism in humans, Neurochem. Int. 43 (4–5) (2003) 323–329.
[72] W.A. Anderson, R. Freeman, Influence of a second radiofrequency field on high-resolution nuclear magnetic resonance spectra, J. Chem. Phys. 37 (1) (1962) 85.
[73] A.J. Shaka, J. Keeler, R. Freeman, Evaluation of a new broad-band decoupling sequence – Waltz-16, J. Magn. Reson. 53 (2) (1983) 313–340.
[74] A.J. Shaka, J. Keeler, Broadband spin decoupling in isotropic liquids, Prog. Nucl. Mag. Res. Sp. 19 (1987) 47–129.
[75] M.H. Levitt, R. Freeman, Composite pulse decoupling, J. Magn. Reson. 43 (3) (1981) 502–507.
[76] M.H. Levitt, Symmetrical composite pulse sequences for Nmr population-inversion .1. Compensation of radiofrequency field inhomogeneity, J. Magn. Reson. 48 (2) (1982) 234–264.
[77] M.H. Levitt, Symmetrical composite pulse sequences for Nmr population-inversion .2. Compensation of resonance offset, J. Magn. Reson. 50 (1) (1982) 95–110.
[78] R.A. de Graaf, Theoretical and experimental evaluation of broadband decoupling techniques for in vivo nuclear magnetic resonance spectroscopy, Magn. Reson. Med. 53 (6) (2005) 1297–1306.
[79] S.Z. Li, J. Yang, J. Shen, Novel strategy for cerebral C-13 MRS using very low RF power for proton decoupling, Magn. Reson. Med. 57 (2) (2007) 265–271.
[80] Y. Xiang, J. Shen, Windowed stochastic proton decoupling for in vivo C-13 magnetic resonance spectroscopy with reduced RF power deposition, J. Magn. Reson Imaging 34 (4) (2011) 968–972.
[81] R. Gruetter, G. Adriany, H. Merkle, P.M. Andersen, Broadband decoupled, H-1-localized C-13 MRS of the human brain at 4 Tesla, Magn. Reson. Med. 36 (5) (1996) 659–664.
[82] J. Shen, K.F. Petersen, K.L. Behar, P. Brown, T.W. Nixon, G.F. Mason, O.A. Petroff, G.I. Shulman, R.G. Shulman, D.L. Rothman, Determination of the rate of the glutamate/glutamine cycle in the human brain by in vivo 13C NMR, Proc. Natl. Acad. Sci. U. S. A. 96 (14) (1999) 8235–8240.
[83] W.P. Aue, S. Muller, J. Seelig, Localized C-13 Nmr-spectra with enhanced sensitivity obtained by volume-selective excitation, J. Magn. Reson. 61 (2) (1985) 392–395.
[84] P.G. Henry, I. Tkac, R. Gruetter, 1H-localized broadband 13C NMR spectroscopy of the rat brain in vivo at 9.4 T, Magn. Reson. Med. 50 (4) (2003) 684–692.
[85] D.P. Burum, R.R. Ernst, Net polarization transfer via a J-ordered state for signal enhancement of low-sensitivity nuclei, J. Magn. Reson. 39 (1) (1980) 163–168.
[86] D.M. Doddrell, D.T. Pegg, M.R. Bendall, Distortionless enhancement of Nmr signals by polarization transfer, J. Magn. Reson. 48 (2) (1982) 323–327.
[87] R.A. De Graaf, In Vivo NMR Spectroscopy – 2nd Edition: Principles and Techniques, John Wiley & Sons, Ltd, 2007, p. 592.
[88] S.R. Hartmann, E.L. Hahn, Nuclear double resonance in the rotating frame, Phys. Rev. 128 (1962) 2042–2053.
[89] R.A. de Graaf, D.L. Rothman, K.L. Behar, State of the art direct 13C and indirect 1H-[13C] NMR spectroscopy in vivo. A practical guide, NMR Biomed. 24 (8) (2011) 958–972.
[90] W. Chen, G. Adriany, X.H. Zhu, R. Gruetter, K. Ugurbil, Detecting natural abundance carbon signal of NAA metabolite within 12-cm(3) localized volume of human brain using H-1-{C-13} NMR spectroscopy, Magn. Reson. Med. 40 (2) (1998) 180–184.
[91] D.L. Rothman, K.L. Behar, H.P. Hetherington, J.A. den Hollander, M.R. Bendall, O.A. Petroff, R.G. Shulman, 1H-Observe/13C-decouple spectroscopic measurements of lactate and glutamate in the rat brain in vivo, Proc. Natl. Acad. Sci. U. S. A. 82 (6) (1985) 1633–1637.
[92] F. Boumezbeur, L. Besret, J. Valette, F. Vaufrey, P.G. Henry, V. Slavov, E. Giacomini, P. Hantraye, G. Bloch, V. Lebon, NMR measurement of brain oxidative metabolism in monkeys using 13C-labeled glucose without a 13C radiofrequency channel, Magn. Reson. Med. 52 (1) (2004) 33–40.
[93] F. Boumezbeur, L. Besret, J. Valette, M.C. Gregoire, T. Delzescaux, R. Maroy,

F. Vaufrey, P. Gervais, P. Hantraye, G. Bloch, V. Lebon, Glycolysis versus TCA cycle in the primate brain as measured by combining 18F-FDG PET and 13C-NMR, J. Cereb. Blood Flow Metab. 25 (11) (2005) 1418–1423.
[94] M.M. Chaumeil, J. Valette, M. Guillermier, E. Brouillet, F. Boumezbeur, A.S. Herard, G. Bloch, P. Hantraye, V. Lebon, Multimodal neuroimaging provides a highly consistent picture of energy metabolism, validating 31P MRS for measuring brain ATP synthesis, Proc. Natl. Acad. Sci. U. S. A. 106 (10) (2009) 3988–3993.
[95] J. Valette, M. Chaumeil, M. Guillermier, G. Bloch, P. Hantraye, V. Lebon, Diffusion-weighted NMR spectroscopy allows probing of 13C labeling of glutamate inside distinct metabolic compartments in the brain, Magn. Reson. Med. 60 (2) (2008) 306–311.
[96] Chen CN, Hoult DI. Biomedical magnetic resonance technology Bristol: Adam Hilger; 1989.
[97] G. Adriany, R. Gruetter, A half-volume coil for efficient proton decoupling in humans at 4 Tesla, J. Magn. Reson. 125 (1) (1997) 178–184.
[98] P.A. Bottomley, C.J. Hardy, P.B. Roemer, O.M. Mueller, Proton-decoupled, overhauser-enhanced, spatially localized C-13 spectroscopy in humans, Magn. Reson. Med. 12 (3) (1989) 348–363.
[99] A. Kumar, P.A. Bottomley, Optimized quadrature surface coil designs, Magn. Reson Mater. Phys. 21 (1–2) (2008) 41–52.
[100] E.S. Roig, A.W. Magill, G. Donati, M. Meyerspeer, L. Xin, O. Ipek, R. Gruetter, A double-quadrature radiofrequency coil design for proton-decoupled carbon-13 magnetic resonance spectroscopy in humans at 7T, Magn. Reson. Med. 73 (2) (2015) 894–900.
[101] M. Meyerspeer, E.S. Roig, R. Gruetter, A.W. Magill, An improved trap design for decoupling multinuclear RF coils, Magn. Reson. Med. 72 (2) (2014) 584–590.
[102] M. Alecci, S. Romanzetti, J. Kaffanke, A. Celik, H.P. Wegener, N.J. Shah, Practical design of a 4 Tesla double-tuned RF surface coil for interleaved H-1 and Na-23 MRI of rat brain, J. Magn. Reson. 181 (2) (2006) 203–211.
[103] A. Dabirzadeh, M.P. McDougall, Trap design for insertable second-nuclei radiofrequency coils for magnetic resonance imaging and spectroscopy, Concept Magn. Reson B 35B (3) (2009) 121–132.
[104] L. Darrasse, J.C. Ginefri, Perspectives with cryogenic RF probes in biomedical MRI, Biochimie 85 (9) (2003) 915–937.
[105] M. Sack, F. Wetterling, A. Sartorius, G. Ende, W. Weber-Fahr, Signal-to-noise ratio of a mouse brain 13C CryoProbe T system in comparison with room temperature coils: spectroscopic phantom and in vivo results, NMR Biomed. 27 (6) (2014) 709–715.
[106] J.T. Vaughan, H.P. Hetherington, J.O. Otu, J.W. Pan, G.M. Pohost, High-frequency volume coils for clinical Nmr imaging and spectroscopy, Magn. Reson. Med. 32 (2) (1994) 206–218.
[107] J.T. Vaughan, G. Adriany, M. Garwood, E. Yacoub, T. Duong, L. DelaBarre, P. Andersen, K. Ugurbil, Detunable transverse electromagnetic (TEM) volume coil for high-field NMR, Magn. Reson. Med. 47 (5) (2002) 990–1000.
[108] R. Gruetter, C. Boesch, M. Muri, E. Martin, K. Wuthrich, A simple design for a double-tunable probe head for imaging and spectroscopy at high fields, Magn. Reson. Med. 15 (1) (1990) 128–134.
[109] S. Li, Y. Zhang, S. Wang, M.F. Araneta, C.S. Johnson, Y. Xiang, R.B. Innis, J. Shen, 13C MRS of occipital and frontal lobes at 3 T using a volume coil for stochastic proton decoupling, NMR Biomed. 23 (8) (2010) 977–985.
[110] J.L.W. Pan, G.F. Mason, J.T. Vaughan, W.J. Chu, Y.T. Zhang, H.P. Hetherington, C-13 editing of glutamate in human brain using J-refocused coherence transfer spectroscopy at 4.1 T, Magn. Reson. Med. 37 (3) (1997) 355–358.
[111] G.F. Mason, J.W. Pan, W.J. Chu, B.R. Newcomer, Y.T. Zhang, R. Orr, H.P. Hetherington, Measurement of the tricarboxylic acid cycle rate in human grey and white matter in vivo by H-1-[C-13] magnetic resonance spectroscopy at 4.1T, J. Cereb. Blood Flow Metab. 19 (11) (1999) 1179–1188.
[112] B. Tiret, A.A. Shestov, J. Valette, P.G. Henry, Metabolic modeling of dynamic (13)C NMR isotopomer data in the brain in vivo: fast screening of metabolic models using automated generation of differential equations, Neurochem. Res. 40 (12) (2015) 2482–2492.
[113] M.M. Dehghani, B. Lanz, J.M. Duarte, N. Kunz, R. Gruetter, Refined analysis of brain energy metabolism using in vivo dynamic enrichment of 13C multiplets, ASN Neuro 8 (2) (2016).
[114] S.W. Provencher, Estimation of metabolite concentrations from localized in vivo proton NMR spectra, Magn. Reson. Med. 30 (6) (1993) 672–679.
[115] P.G. Henry, M. Marjanska, J.D. Walls, J. Valette, R. Gruetter, K. Ugurbil, Proton-observed carbon-edited NMR spectroscopy in strongly coupled second-order spin systems, Magn. Reson. Med. 55 (2) (2006) 250–257.
[116] P.G. Henry, G. Oz, S. Provencher, R. Gruetter, Toward dynamic isotopomer analysis in the rat brain in vivo: automatic quantitation of 13C NMR spectra using LCModel, NMR Biomed. 16 (6–7) (2003) 400–412.
[117] D.K. Deelchand, K. Ugurbil, P.G. Henry, Investigating brain metabolism at high fields using localized 13C NMR spectroscopy without 1H decoupling, Magn. Reson. Med. 55 (2) (2006) 279–286.
[118] L. Vanhamme, S. Van Huffel, P. Van Hecke, D. van Ormondt, Time-domain quantification of series of biomedical magnetic resonance spectroscopy signals, J. Magn. Reson. 140 (1) (1999) 120–130.
[119] B. Lanz, J.M. Duarte, N. Kunz, V. Mlynarik, R. Gruetter, C. Cudalbu, Which prior knowledge? Quantification of in vivo brain 13C MR spectra following 13C glucose infusion using AMARES, Magn. Reson. Med. 69 (6) (2013) 1512–1522.
[120] O. Henriksen, In vivo quantitation of metabolite concentrations in the brain by means of proton MRS, NMR Biomed. 8 (4) (1995) 139–148.
[121] R. Buchli, E. Martin, P. Boesiger, Comparison of calibration strategies for the in vivo determination of absolute metabolite concentrations in the human brain by 31P MRS, NMR Biomed. 7 (5) (1994) 225–230.
[122] R. Gruetter, E.R. Seaquist, K. Ugurbil, A mathematical model of compartmentalized neurotransmitter metabolism in the human brain, Am. J. Physiol. Endocrinol. Metab. 281 (1) (2001) E100–E112.
[123] P.G. Henry, G. Adriany, D. Deelchand, R. Gruetter, M. Marjanska, G. Oz, E.R. Seaquist, A. Shestov, K. Ugurbil, In vivo 13C NMR spectroscopy and metabolic modeling in the brain: a practical perspective, Magn. Reson. Imaging 24 (4) (2006) 527–539.
[124] J. Kurhanewicz, R. Bok, S.J. Nelson, D.B. Vigneron, Current and potential applications of clinical 13C MR spectroscopy, J. Nucl. Med. 49 (3) (2008) 341–344.
[125] K.M. Brindle, S.E. Bohndiek, F.A. Gallagher, M.I. Kettunen, Tumor imaging using hyperpolarized 13C magnetic resonance spectroscopy, Magn. Reson. Med. 66 (2) (2011) 505–519.
[126] D.M. Wilson, J. Kurhanewicz, Hyperpolarized 13C MR for molecular imaging of prostate cancer, J. Nucl. Med. 55 (10) (2014) 1567–1572.
[127] M.M. Chaumeil, P.E. Larson, H.A. Yoshihara, O.M. Danforth, D.B. Vigneron, S.J. Nelson, R.O. Pieper, J.J. Phillips, S.M. Ronen, Non-invasive in vivo assessment of IDH1 mutational status in glioma, Nat. Commun. 4 (2013) 2429.